of 0.229 (40 to 2.1 Å) (12). Packing of subunits within the crystal defined an unambiguous interface through which the β subunit and T1 tetramers interact: The large flat surface of β engages four prominent loops (contact loops) extending from the NH$_2$-terminal side of the T1 tetramer (Fig. 1).

Comparison of the isolated T1 and β subunit structural models with their counterparts in the complex reveals only small differences. One of these is a slight tilt of the T1 domain subunits with respect to the central four-fold axis (4). The tilt results in a separation of the subunits at the COOH-terminal side, widening the aperture, and a constriction at the NH$_2$-terminal side where T1 contacts the β subunit.

To confirm this complex in vivo, we studied the interaction of α and β subunits in *Xenopus* oocytes by measuring inactivation, which refers to occlusion of the pore by an inactivation peptide (Fig. 2A) (6, 10). The inactivation peptide is effective when attached to the NH$_2$-terminus of either the α or β subunits (Fig. 2B), apparently because the attachment sites are very near each other in the T1$_4$β$_4$ complex (Fig. 1C). Thus, if the α subunit does not have its own inactivation peptide, trans-inactivation caused by a β subunit indicates α-β subunit association. Following a described method (10), a Kv1.4 K$^+$ channel without an inactivation gate (Kv1.4-IR) was coexpressed with the β2 subunit containing an inactivation gate (β12 chimera) (Fig. 2) (13). The T1 domain of Kv1.4 is 85% identical to that of

Kv1.1 used in the structure determination.

When the T1 domain is removed from the Kv1.4-IR channel by means of genetic deletion (13) (residues 2 to 278), inactivation is not observed in the presence of the β12 chimera (Fig. 2C), implying that the T1 domain is necessary for β subunit association. The occurrence of inactivation when the inactivation peptide is on the channel's own NH$_2$-terminus, even in the absence of a T1 domain, demonstrates that the inactivation process itself does not require a T1 domain [Fig. 2C; see also (14)]. Thus, the T1 domain does not participate directly in inactivation but serves to hold the β subunit in place.

To determine which amino acids are important for T1$_4$β$_4$ complex formation in vivo, we made single-site alterations (13). On the T1 domain, only mutations involving contact loop residues abolish inactivation (Fig. 2, D and E). The effect of the point mutations is most compatible with disruption of β subunit binding to the α subunit: The same mutations do not interfere with inactivation caused by a gate on the NH$_2$-terminus of the α subunit (15). On the β subunit, single-site mutations affect inactivation only when introduced onto the surface where the T1 contact loops touch the β subunit in the crystal structure (Fig. 2, D and E).

Certain mutations on the β subunit [e.g., Met^{196} → Trp (M196W)] reduce the extent of inactivation but do not abolish it (Fig. 2D). In such cases, the inactivating component exhibits wild-type kinetics, implying that only a fraction of channels contain a β sub-

unit because the mutant β subunit has a reduced affinity for the α subunit. The possibility of insufficient mutant β subunit expression, resulting in a mismatch between the numbers of β and α subunits, is excluded by a control experiment. Mutation M196W on the β subunit rescues the loss of inactivation caused by T1 contact loop mutation Phe^{214} → Val (F214V) (Fig. 2D). This result offers very strong support for the crystallographically defined structure in the context of a living cell. The conclusion that the T1 contact loops provide the β subunit docking surface offers insight into the specificity of α-β subunit assembly: The amino acid sequence of the T1 contact loop is highly conserved within a given family of K$^+$ channels but not between members of different families. Thus, β1 and β2 subunits associate with Kv1 but not Kv2 K$^+$ channels (16).

The aqueous channel down the center of the T1$_4$β$_4$ complex is too narrow (~4 Å and positively charged) to allow entry of tetraethylammonium, a pore-blocking cation, or the inactivation peptide (Fig. 3). If not through the center of the T1$_4$β$_4$ complex, how does the ion pathway connect to the cytoplasm? We addressed this question by again exploiting inactivation. Inactivation occurs when an inactivation peptide binds at or near the pore (Fig. 2A). Electrostatic interactions help to mediate this process: Mutations of basic (positive charged) amino acids on the inactivation peptide influence the rate and extent of inactivation (17). Therefore, we expect to find complementary acidic (neg-

Fig. 1. Structure of the T1$_4$β$_4$ complex. (**A**) Ribbon representation showing four contact loops that form the primary interface between the T1 and β tetramers. The T1 tetramer is red and the β tetramer is blue. (**B**) Molecular detail of a T1 contact loop touching the β subunit surface (24). (**C**) Stereoview of a Cα trace of the β tetramer (blue) and T1 tetramer (red) viewed along the fourfold axis and showing the relative proximity of the NH$_2$-termini of each where inactivation gates are attached. The NADP$^+$ cofactor in each active site is green. This figure was generated with the programs O (25), MOLSCRIPT (26), Raster-3D (27), and POVRAY (28).
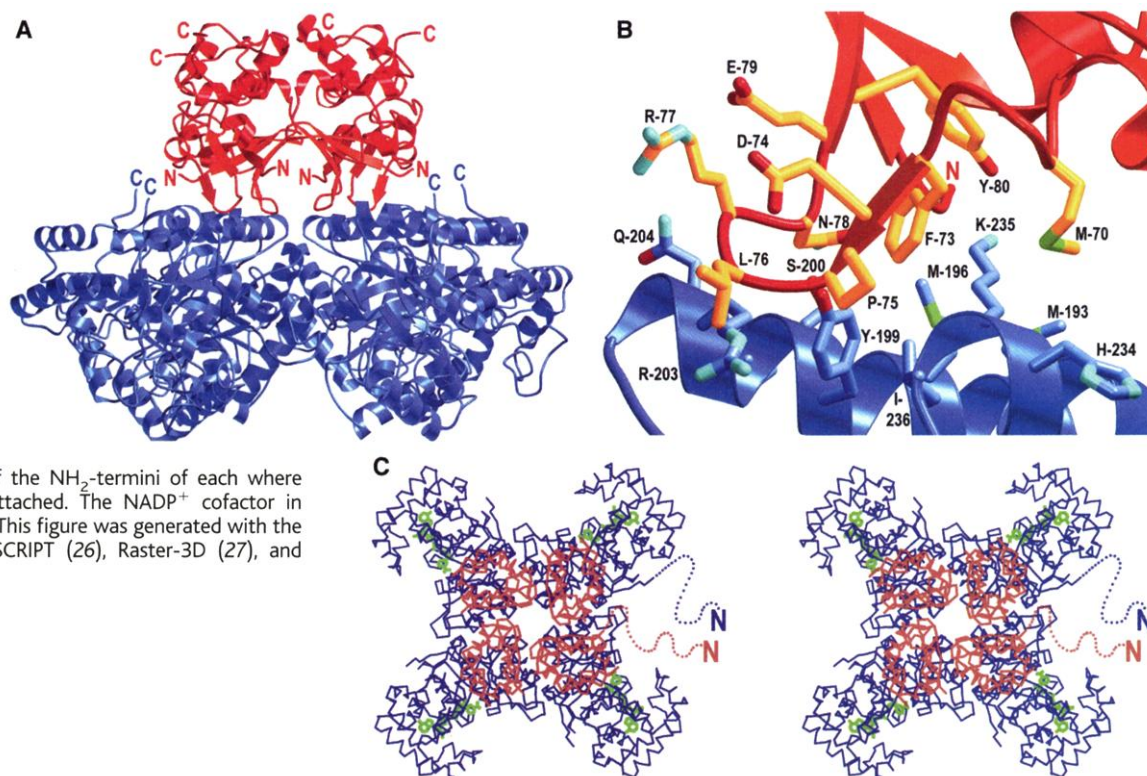
ative charged) amino acids on the channel near the inactivation peptide–binding site. The T1-S1 linker (connecting T1 to the first membrane-spanning segment) contains several acidic amino acids. When three of these residues, located six amino acids COOH-terminal to the T1 structure (Glu[273], Asp[274], and Glu[275] in Kv1.4), are mutated to Ala (neutral) or Lys (positive), the rates of inactivation and recovery from inactivation are affected (18) (Fig. 4, A and B), and mutations to Lys (negative to positive) have the largest influence. Mutation of Val[247] to Lys (neutral to positive) also reduced the rate of inactivation (Fig. 4C). Val[247] is located on the surface of the T1 domain close to where the T1-S1 linker emerges (Fig. 5).

Mutations were also made in the inactivation peptide to reduce its positive charge. These mutations affected inactivation, but more importantly their influence depended on the charge at positions 273 to 275 in the T1-S1 linker. Thus, mutations in the inactivation peptide are coupled in mutant cycle analysis to mutations in the T1-S1 linker near the T1 domain (Fig. 4C) (19). In order for such coupling to occur, the peptide must be near the T1-S1 linker when it inactivates the pore. Because the peptide cannot fit through the center of the $T1_4\beta_4$ complex, it must reach the pore by entering lateral openings above the T1 tetramer (Fig. 5).

The structure of the T1 domain tetramer seemed to be inconsistent with several decades of K^+ channel pharmacology: The central hole is too narrow for many of the classical organic blocking agents (4). When the T1 domain was deleted from the α subunit, the single channel conductance did not change substantially, as if the T1 tetramer does not form an extension of the pore (20). Thus, it was proposed that either the T1 domain is not a tetramer in the context of the integral membrane channel or that ions move between the cytoplasm and pore through an alternative pathway.

The data presented here establish that the T1 domain is indeed a tetramer in the K^+
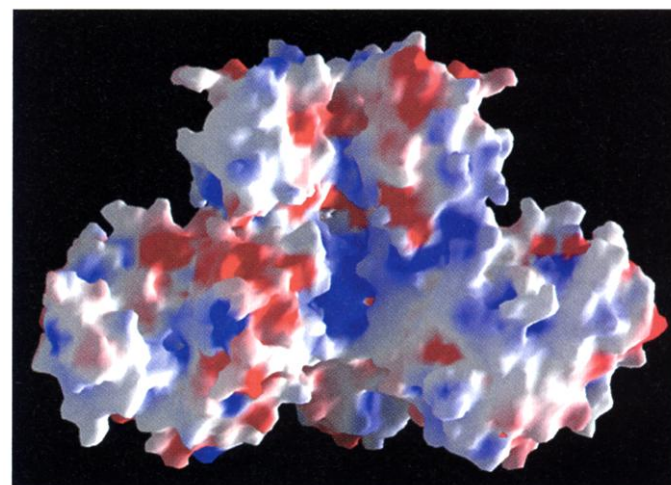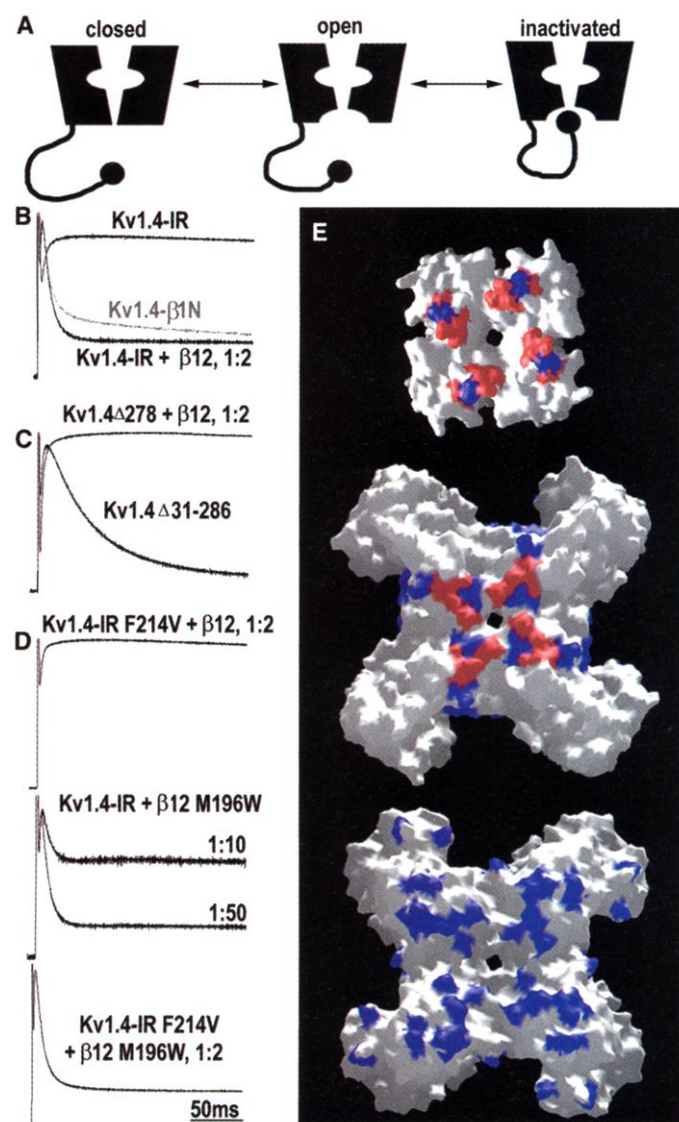
Fig. 2 (left). Functional analysis of the $T1_4\beta_4$ interface. (A) Illustration of N-type K^+ channel inactivation. The black circle represents the inactivation peptide. (B) Potassium currents recorded from *Xenopus* oocytes under voltage clamp containing channels without an inactivation peptide (Kv1.4-IR) or with an inactivation peptide attached to the NH_2-terminus of the α subunit (Kv1.4-β1N) or β subunit (Kv1.4-IR + β12). The α and β subunits were coexpressed at an RNA ratio of 1:2 (v:v) (13). (C) The Kv1.4Δ278 channel lacks amino acids 2 to 278, which make up Kv1.4 channel's own inactivation peptide and T1 domain. The β12 chimera fails to cause inactivation (Kv1.4Δ278 + β12). The Kv1.4Δ31-286 channel (amino acids 31 to 286 deleted) lacks a T1 domain but contains its own inactivation peptide (Kv1.4Δ31-286), which differs from that of β12, accounting for the slower inactivation rate. (D) (Top) A point mutation on the contact loop of the T1 domain (Kv1.4-IR F214V) prevents β12 chimera–induced inactivation (residue Phe[73] in Kv1.1) (Middle) Currents carried by Kv1.4-IR channels expressed with a mutant β subunit (β12 M196W) at two RNA volume ratios, 1:10 and 1:50, undergo incomplete inactivation. (Bottom) Coexpression of Kv1.4-IR F214V mutant α subunit and β12 M196W mutant β subunit yields inactivation properties similar to the combination of wild-type α and β subunits. In all recordings, oocytes were held at −80 mV and stepped to +60 mV for 200 ms. (E) GRASP view of T1 and β2 subunits showing the effect of selected point mutations on channel inactivation (red, alteration; blue, no alteration). (Top) NH_2-terminal surface of the T1 domain. Red residues are Phe[73], Leu[76], and Arg[78], and the blue residue is Pro[75]. (Middle) Flat surface of the Kvβ2 subunit. Red residues are Met[196], Tyr[199], Ser[200], and Gln[204], and blue residues are Arg[203], Lys[268], Lys[129], and Met[193]. (Bottom) Concave surface of the β subunit. Blue residues are Asp[66], Asp[67], Tyr[90], Lys[104], Lys[105], Lys[106], Lys[124], Glu[145], Gln[148], Glu[150], Asn[158], Arg[159], Arg[189], Pro[260], and Pro[261]. This figure was made with GRASP (29). **Fig. 3 (right).** The central pore of the $T1_4\beta_4$ complex. A molecular surface calculated over three of the four T1-β subunits reveals a central pore with unusual internal electrostatic features. The pore is coincident with the molecular four-fold axis and extends the length of the complex. At its apex, it is sufficiently wide to permit the entry of ions. The inner surface of this cavity is lined with charged amino acid side chains that are conserved in the Kv1 family. Calculation of the electrostatic potential was carried out at an ionic strength equivalent to 0.15 M KCl. Dielectric constants of 2.0 for the protein interior and 80.0 for solvent were used. Regions of the molecular surface exhibiting intense negative charge are colored red, and electropositive regions are colored blue. This figure was generated with the program GRASP (29).

Fig. 4. Evidence for pore openings above the T1 domain. (**A**) (Top) β12 chimera–induced inactivation of wild-type Kv1.4-IR α subunits (WT) and α subunits with Ala (A) or Lys (K) substituted at positions 273 to 275. (Bottom) Currents from wild-type α subunits (WT) or α subunits with Ala substituted at 273 to 275 (A) coexpressed with the β12 chimera containing a wild-type inactivation gate (+β12) or K13N, R15G mutant inactivation gate (+1315NG). The experimental conditions were identical to those described in Fig. 2D. (**B**) (Top) Rate of recovery from inactivation measured in paired pulses from a holding voltage of −80 mV and stepping the membrane to +60 mV. The initial conditioning pulse was 400 ms. The dashed curve corresponds to an exponential function ($\tau = 11$ s) fitted to the envelope defined by the peak current of the test pulse. (Bottom) Fraction of recovery as a function of time between the conditioning pulse and the test pulse. ■, Kv1.4-IR α subunit paired with the β12 chimera; ●, α subunit with Ala substituted at 273 to 275 coexpressed with β12 chimera; ○, α subunit with Lys substituted at 273 to 275 coexpressed with β12 chimera. The solid lines are single exponential fits. Error bars are the standard error of the mean (SEM) from ≥five independent experiments. (**C**) Double-mutant cycle analysis of inactivation. The time constants of inactivation (τ_{inac}) and recovery (τ_{rec}) and the ratio between these two time constants are tabulated (±SEM, ≥five independent experiments) (*18*). The Ω value was calculated as described (*19*).

	τ_{inac} (ms)	τ_{rec} (sec)	K_d (τ_{inac}/τ_{rec}) *10^3	Ω
Kv1.4-IR + β12	5.0 ± 0.3	11 ± 0.7	0.45	
Kv1.4-IR + β12 (R20Q)	8.1 ± 0.6	7.7 ± 0.4	1.1	
Kv1.4-IR + β12 (1315NG)	23 ± 1	8.3 ± 0.4	2.8	
Kv1.4-IR (A)+ β12	26 ± 2	4.8 ± 0.3	5.4	
Kv1.4-IR (A) + β12 (R20Q)	27 ± 2	8.3 ± 0.5	3.3	4.0
Kv1.4-IR (A) + β12 (1315NG)	45 ± 3	4.3 ± 0.2	10	3.4
Kv1.4-IR (K) + β12	45 ± 3	3.8 ± 0.3	12	
Kv1.4-IR (K)+ β12 (R20Q)	50 ± 4	2.8 ± 0.2	18	1.6
Kv1.4-IR (K)+ β12 (1315NG)	40 ± 3	3.1 ± 0.3	13	5.7
Kv1.4-IR (V247K) + β12	19 ± 0.9	1.5 ± 0.1	13	
Kv1.4-IR (V247K) + β12 (R20Q)	24 ± 1.1	0.9 ± 0.08	26	1.2
Kv1.4-IR (V247K) + β12 (1315NG)	45 ± 1.5	0.83 ± 0.09	54	1.5

Fig. 5. Composite model of a voltage-dependent K$^+$ channel. The α subunit is shown in red, and the β subunit is in blue. The model of the pore region is based on the KcsA K$^+$ channel (*30*). The structures of the voltage-sensing region and connectors are unknown (depicted schematically). An NH$_2$-terminal inactivation peptide is shown entering a lateral opening to gain access to the pore. Proposed locations of amino acids 273 to 275 on the T1-S1 linker are shown (black asterisks) with the location of Val^{247} on the T1 domain surface (green asterisks).
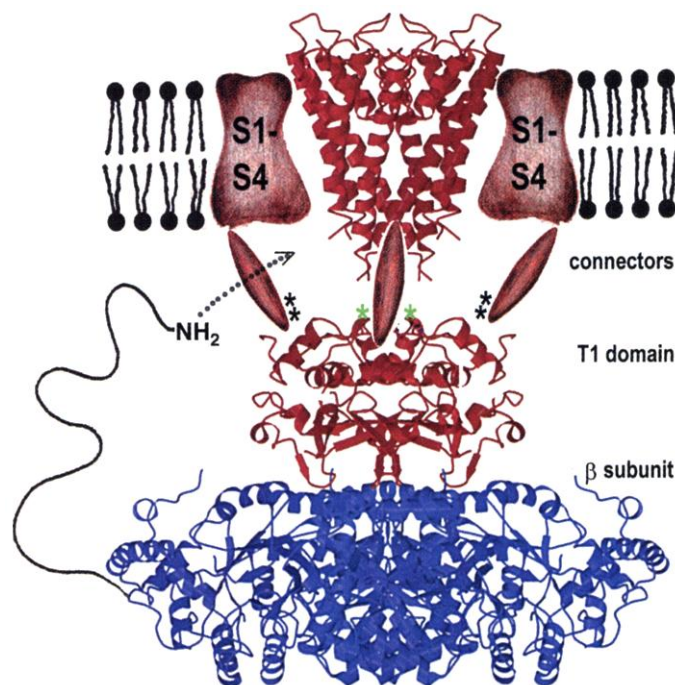
channel and that the T1 domain tetramer forms the docking platform for the β subunit. The contact loops extending from the NH$_2$-terminal face of the T1 domain are obvious structures for interfacing with intracellular proteins—in this case the β subunit. We suggest that the major role of the T1 domain is to form a docking site for proteins whose activities are coupled to K$^+$ channel function.

The apparent paradox of a too narrow pore in the T1 domain has a simple explanation. Our data suggest the presence of lateral openings between the T1 domain and the integral membrane part of the α subunit (Fig. 5). This explanation accounts for the interaction between the inactivation peptide and amino acids on the top (COOH-terminal face) of T1 and in the T1-S1 linker close to T1. Because the peptide must access the pore through lateral openings, K$^+$ ions must also pass through the openings. Lateral openings in the cytoplasm, with negative charged amino acids, are also a structural feature of nicotinic acetylcholine receptor ion channels (*21*).

A single inactivation gate binds to its receptor near the intracellular pore entryway in an exclusive fashion when inactivation occurs (*22*,

23). Our findings are entirely consistent with this conclusion. Although we expect there to be four openings above the T1 domain, there is presumably only one site near the pore entryway where a single peptide can induce inactivation. We propose that the inactivation peptide is poorly structured and snakes its way into a lateral opening to reach the central pore and this is why mutations in the T1-S1 linker influence the process. In some cases, four peptides may even be bound above T1, poised and ready, before inactivation.

The central question as to why K^+ channels contain an oxido-reductase enzyme subunit remains unanswered. In this report, we have shown how the β subunit attaches to a voltage-dependent K^+ channel through its interaction with the T1 domain. We previously suggested that interactions between α and β subunits may allow cellular redox regulation of the channel or channel regulation of enzyme activity (1). The structure of the $T1_4\beta_4$ complex takes us one step closer to understanding how such energetic coupling might occur.

References and Notes

1. J. M. Gulbis, S. Mann, R. MacKinnon, *Cell* **97**, 943 (1999).
2. G. Shi *et al.*, *Neuron* **16**, 843 (1996).
3. N. Nagaya and D. M. Papazian, *J. Biol. Chem.* **272**, 3022 (1997).
4. A. Kreusch, P. J. Pfaffinger, C. F. Stevens, S. Choe, *Nature* **392**, 945 (1998).
5. C. M. Armstrong, *J. Gen. Physiol.* **58**, 413 (1971).
6. W. N. Zagotta, T. Hoshi, R. W. Aldrich, *Science* **250**, 568 (1990).
7. S. D. Demo and G. Yellen, *Neuron* **7**, 743 (1991).
8. S. Sewing, J. Roeper, O. Pongs, *Neuron* **16**, 455 (1996).
9. W. Yu, J. Xu, M. Li, *Neuron* **16**, 441 (1996).
10. J. Rettig *et al.*, *Nature* **369**, 289 (1994).
11. A. Baumann, A. Grupe, A. Ackermann, O. Pongs, *EMBO J.* **7**, 2457 (1988).
12. DNA encoding the NH₂-terminal cytoplasmic T1 domain (residues 1 to 135) of the rat Kv1.1 α subunit was subcloned into a pAcG2T (Pharmingen) baculovirus transfer vector as a glutathione S-transferase (GST) fusion construct with Bam HI and Eco RI restriction sites. DNA encoding residues 36 to 367 of rat Kvβ2 was subcloned into pFastBac1 (Gibco) between Bam HI and Eco RI restriction sites. For coexpression, cells were infected with two viruses. At 72 hours, cells were harvested by centrifugation and resuspended in a cold buffer (I) comprising 20 mM tris-Cl (pH 8.0), 150 mM KCl, 5 mM MgCl₂, and 5 mM dithiothreitol. Phenylmethylsulfonyl fluoride was added to 1 mM, and the cells were promptly lysed with a French pressure cell. After adding deoxyribonuclease, the lysate was incubated for 20 min on ice and then centrifuged to pellet cellular debris. The filtered lysate was incubated with glutathione sepharose 4B beads (Pharmacia) for 2 hours at 4°C. Proteolytic (thrombin) removal of the GST tag was preceded by extensive washing of the matrix-bound material with a buffer (II) containing 20 mM tris-Cl (pH 8.0), 150 mM KCl, and 2 mM CaCl₂. The cleaved protein was eluted, concentrated, and loaded onto a size-exclusion (Superdex-200 10/30; Pharmacia) column equilibrated in buffer (I). Peak fractions corresponding to a heterooctamer (T1₄β₄) were pooled and cleaved with trypsin, yielding a T1(27-129)₄β₄ octamer. Size exclusion was used as a final purification step. Column fractions corresponding to heterooctameric complex were collected, pooled, and concentrated to 15 mg/ml. Tetragonal crystals containing a single T1β heterodimer (P4₂₁2; $a = 100.7$ Å, $c = 110.9$ Å) grew in hanging drops; 1 μl of the protein solution was mixed with 1 μl of a reservoir solution containing 50 mM glycine (pH 8.6) and 6% PEG400 and allowed to equilibrate by vapor diffusion. Crystals were cryoprotected by transfer into a similar solution containing 25% glycerol, mounted in nylon loops, and frozen in propane. Diffraction data to 2.1 Å were collected from single plates at beamlines A1 (CHESS) and X25 (Brookhaven NSLS) with charge-coupled device detectors. Images were processed with DENZO and intensities were merged with SCALEPACK [Z. Otwinowski, in *Proceedings of the CCP4 Study Weekend* (SERC Daresbury Laboratory, Warrington, UK, 1993), pp. 56–62; Z. Otwinowski and W. Minor, *Methods Enzymol.* **276**, 307 (1997)]. A set of 400,177 measured reflections (33,907 unique) in the resolution range 40.0 to 2.1 Å gave a 98.8% complete data set (92.9% in the outer shell; 2.15 to 2.10 Å). The overall agreement factor R_{merge} (on intensity) is 8.0% (30.0% in the outer shell). The average intensity/standard deviation is 17.8 (4.3 in the outer shell). The T1₄β₄ structure was solved by molecular replacement with AMORE [J. Navaza, *Acta Crystallogr. Sect. A* **50**, 157 (1994)]. A refined model of the conserved core of rat Kvβ2 (1qrq; residues 36 to360) was used to initiate rotation and translation searches in the resolution range 8.0 to 4.0 Å. A peak 8.8σ above the mean was the highest in the rotation function. Translation searches yielded a peak at 18.0σ. Cycles of rigid body refinement of the heterodimer with data between 8.0 and 4.0 Å reduced the R factor to 0.393 and gave a correlation coefficient of 57.7. Before refinement, all temperature factors were fixed at 30 Å², and several residues in mobile regions together with several side chains were deleted from the model. The β subunit T1 complex model was then refined by minimization and simulated annealing procedures with the maximum likelihood target implemented in CNS [A. T. Brunger *et al.*, *Crystallogr. D. Biol. Crystallogr.* **54** (part 5), 905 (1998)]. $3F_o − 2F_c$ (where F_o and F_c are the observed and calculated structure factors, respectively) maps were calculated on the basis of an average of 10 refined structures and were of sufficiently high quality to enable almost complete tracing of the T1 domain. A number of cycles of building and refinement were required to place the remainder of the structure. All data falling between resolution limits of 40.0 and 2.1 Å, with the exception of a random 5% used for calculation of the R_{free}, were used in the refinement. Bulk solvent and anisotropic temperature factor corrections (final anisotropic tensor elements: B11, 0.26 Å²; B22, 0.26 Å²; and B33, −0.52 Å²) were applied to the reflection data. The crystallographic R_{free} was monitored to reduce model bias. Individual temperature factors were refined for all nonhydrogen atoms. The refined model has good geometry with one Ramachandran outlier near NADP and contains 418 residues and 1 nicotinamide adenine dinucleotide phosphate (NADP⁺) and 267 water molecules and has an R_{free} of 0.229 and an R_w of 0.211. Six residues at the COOH-terminus of the β subunit, eight at the NH₂-terminus of T1, and three at the COOH-terminus of T1 were omitted from the model because of weak electron density in the region. Side chains were not modeled beyond the β carbon for the following amino acids: Lys¹²⁴, Lys²⁶⁸, and Ser³⁶¹.
13. The Kv1.4-IR (residues 2 to 110 deleted), Kv1.4Δ278 (residues 2 to 278 deleted), and Kv1.4Δ31-286 (residues 31 to 286 deleted) were generated by the overlapping polymerase chain reaction method. The β12 chimera and the Kv1.4-β1N were made by splicing DNA encoding residues 1 to 70 of β1 onto DNA encoding residues 36 to 366 of β2 or DNA encoding residues 137 to 655 of Kv1.4, respectively. All constructs were cloned into pBluescript KS⁺. Point mutations were made by the QuickChange method (Stratagene) and confirmed by sequencing the entire insertion. RNA was prepared by T7 polymerase transcription and injected into *Xenopus laevis* oocytes [Z. Lu and R. MacKinnon, *J. Gen. Physiol.* **104**, 477 (1994)]. RNA ratios refer to volumes mixed before injection. K^+ currents were recorded under two-electrode voltage clamp (OC725B; Warner Instrument, Hamden, CT). Electrodes were drawn from borosilicate glass capillaries (World Precision Instrument, Sarasota, FL) to a resistance of ~0.5 megaohms (3 M KCl). Bath solution contained 96 mM NaCl, 2 mM KCl, 0.3 mM CaCl₂, 1 mM MgCl₂, and 5 mM Hepes (pH 7.6) with NaOH. Analog data from the amplifier were filtered (2 kHz, −3 dB) with an eight-pole Bessel filter (Frequency Devices, Haverhill, MA), digitized at 10 kHz, and transferred to a computer hard disk with an Axon 1200 digitization board and supporting software (Clampex version 8; Axon Instrument, Foster City, CA).
14. T. E. Lee, L. H. Philipson, D. J. Nelson, *J. Membr. Biol.* **151**, 225 (1996).
15. J. M. Gulbis, M. Zhou, S. Mann, R. MacKinnon, data not shown.
16. K. Nakahira, G. Shi, K. J. Rhodes, J. S. Trimmer, *J. Biol. Chem.* **271**, 7084 (1996).
17. R. D. Murrell-Langnado and R. W. Aldrich, *J. Gen. Physiol.* **102**, 949 (1993).
18. Inactivation time constants were obtained by fitting the current decay with exponential functions with Clampfit (Axon) software. Expression of Kv1.4-IR with β12 chimera yielded two exponentials: a predominant (>90%) fast component (time τ < 60 ms) and a minor (<10%) component (τ ~ 500 ms). The slower time constant was relatively invariable and coincided with the COOH-type inactivation of Kv1.4-IR [S. H. Heinemann, J. Rettig, H. R. Graack, O. Pongs, *J. Physiol.* **493**, 625 (1996)]. In double-mutant cycle analysis, only the predominant component was used. Inactivation recovery was studied with paired pulses (22). The peak of the second pulse in the pair was graphed as a function of time after the first pulse, defining an envelope of recovery that was fit to an exponential function with Origin (Microcol Software, Northampton, MA). Recovery from inactivation for Kv1.4-IR paired with the β12 chimera was well described by single exponential function.
19. The double-mutant cycle parameter

$$\Omega = \frac{K_d^{wt,wt} \times K_d^{mut,mut}}{K_d^{wt,mut} \times K_d^{mut,wt}}$$

was used to quantify the degree of coupling between two mutations [P. Hidalgo and R. MacKinnon, *Science* **268**, 307 (1995)]. Here, K_d refers to a dimensionless parameter defined by the ratio of inactivation and recovery time constants, τ_{inac}/τ_{rec}. Because $\tau_{rec} \gg \tau_{inac}$, K_d is very close to the equilibrium ratio of open to inactivated channels. A value of Ω greater than unity indicates that the effects of two mutations are coupled.
20. W. R. Kobertz and C. Miller, *Nature Struct. Biol.* **6**, 1122 (1999).
21. A. Miyazawa, Y. Fujiyoshi, M. Stowell, N. Unwin, *J. Mol. Biol.* **288**, 765 (1999).
22. R. MacKinnon, R. W. Aldrich, A. W. Lee, *Science* **262**, 757 (1993).
23. F. Gomez-Lagunas and C. M. Armstrong, *Biophys. J.* **68**, 89 (1995).
24. Single-letter abbreviations for the amino acid residues are as follows: A, Ala; C, Cys; D, Asp; E, Glu; F, Phe; G, Gly; H, His; I, Ile; K, Lys; L, Leu; M, Met; N, Asn; P, Pro; Q, Gln; R, Arg; S, Ser; T, Thr; V, Val; W, Trp; and Y, Tyr.
25. T. A. Jones, J. Y. Zou, S. W. Cowan, M. Kjeldgaard, *Acta Crystallogr. Sect. A* **47**, 110 (1991).
26. P. Kraulis, *J. Appl. Crystallogr.* **24**, 946 (1991).
27. D. Bacon and W. F. Anderson, *J. Mol. Graph* **6**, 219 (1988).
28. See www.povray.org.
29. A. Nicholls, K. A. Sharp, B. Honig, *Proteins* **11**, 281 (1991).
30. D. A. Doyle *et al.*, *Science* **280**, 69 (1998).
31. We thank J. Bonnano for technical assistance; J. Morais Cabral, R. Dutzler, Y. Jiang, A. Pico, and Y. Zhou for help with data collection; B. Chait and M. Cadene for mass spectrometry; O. Pongs for Kv1.4 DNA; J. Trimmer for β subunit DNA; members of the MacCHESS (A1) and Brookhaven National Laboratory (X25) staff for assistance in data collection; and W. Chin for artwork and help with the manuscript. The coordinates have been submitted under Protein Data Bank ID code 1EXB. R.M. is an investigator in the Howard Hughes Medical Institute. Supported by NIH grant GM47400.

21 April 2000; accepted 1 June 2000